APPLICATION OF GROUND-PENETRATING RADAR IN THE SUBSURFACE INVESTIGATION OF SILVER LAKE PLAYA IN NORTHWEST NEVADA

By

Andrew W. Gibson

A thesis submitted in partial fulfillment

of the requirements for the degree of

MASTER OF SCIENCE

in

Geosciences

Middle Tennessee State University

May 2022

ACKNOWLEDGEMENTS

First and foremost, I must thank my God for giving me the faith and ability to complete this task. With God, all things are possible.

I must express my most profound appreciation to Dr. Henrique Momm for seeing me through this process and guiding me along the way. You have been a fantastic advisor and a good friend. You are an endless font of relief to myself and my colleagues.

I would also like to thank the members of my advisory committee, Dr. Clay Harris and Dr. Jeremy Aber. Your instruction and advice have been invaluable over the years. I am very grateful for your willingness to participate in this effort.

I would like to thank Dr. Mark Abolins. Thank you for your support and instruction.

I have to thank my colleagues Ben, Brie, Hannah, and Kristie. I am grateful to you all for your support and friendship. We have struggled together, and we are better for it.

Finally, I must thank my wonderful family. God blessed me with an amazing mother and father. You both have been tireless in your support. Your unconditional love, friendship, and endless prayers have seen me through the ups and downs of life, and I owe everything to you both. My son Andrew, you are my light, the reason I am here on this earth. Thank you for being the best son I could ever ask for and my best friend. I am so proud to be your father.

ABSTRACT

The focus of this study is the subsurface characterization of Silver Lake Playa in northwest Nevada, USA, by application of ground-penetrating radar (GPR) and integration of Geographic Information Systems (GIS). The nondestructive nature of GPR analysis is able to keep intact the geomorphological and potential cultural setting of the study area while supporting the selection of appropriate sites for further, more destructive investigations. GPR surveys revealed four distinct radar facies used to describe the subsurface within the study area. GPR datasets correlate with soil samples from auger holes (A1, A3, A5). GPR datasets reveal radar signatures that correlate to other studies of fan delta environments (Roberts et al., 2003). GPR data from the playa-lunette at the southeastern margin of the playa is consistent with other studies of playa-lunette morphology (Twidale, 2015). GPR appears to be an effective means of collecting data in low salinity playa environments.

TABLE OF CONTENTS

LIST OF TABLES

LIST OF FIGURES

LIST OF SYMBOLS AND ABBREVIATIONS

AGC - Automatic Gain Control

^{o}C - Celsius

CSV- Comma Separated Value

g/L - Grams per Liter

GNSS - Global Navigation Satellite System

GPR - Ground-Penetrating Radar

GPS - Global Positioning System

GSD - Grain Size Distribution

HDR - High Dynamic Range

MHz - Megahertz

RDP - Relative Dielectric Permittivity

CHAPTER I

INTRODUCTION

Natural records of climate variability or proxies can aid in developing an understanding of past climatic fluctuations. Perhaps the most crucial repository of climate proxy data related to the middle latitudes, spanning the Last Glacial Maximum until the present, has come from studying the geomorphic evolution of the arid Great Basin of western North America (Cohen et al., 2000). Paleoclimate proxy data for the region indicates that hydroclimate variability was a driving factor in lake-level fluctuation (Bird et al., 2009). Proxy data also presents inconsistencies in sub-basin and paleolake response potentially linked to abrupt climatic changes. Correlating climatic data discovered in playa systems across the Great Basin with paleolake proxy data could support understanding of large-scale climate fluctuations that shaped the region.

Playas

Playas occur in regions of high evaporation and low precipitation. The salinity of the water supply plays a role in playa development as salts affect evaporation rates. Some playas can develop a thick crust as high concentrations of salts lead to the formation of evaporites (Hills, 1940). These highly saline environments are more often associated with playas that have direct groundwater discharge, allowing for capillary action to pull minerals to the surface. Playa surface conditions are generally smooth, hard, and dry in areas where recharge is due to surface runoff. There is always the possibility that a combination of conditions allows for multiple surface types in a single playa environment. Changes in salinity and redistribution of sediments in playas speak to the direct effect climate has on playa evolution. Evidence of climate change in the sedimentary record of playas could serve as proxy data for correlation with other proxy data related to paleoclimate.

Significance and Research Hypothesis

The purpose of this study is to determine if ground-penetrating radar can be used as a non-invasive surveying methodology to characterize sedimentology of playa environments and discover locations for more invasive data collection. Playas not only contain sedimentary records but can be locations of cultural significance. There is evidence that ancient peoples had encampments in these environments (Hurst et al., 2010). If found to be a viable data collection method in playa environments, GPR surveys could retrieve data while preserving site integrity (Fig. 1).

Figure 1. Photograph of what appears to be a spearpoint in the pre-Clovis style, discovered in Silver Lake Playa during a GPR survey.

Geomorphological and sedimentary data collected using geophysical methods could correlate with existing paleoclimate proxy data and aid in investigating late Quaternary climatic fluctuation and the hydrologic response of paleolakes and wetlands of the Great Basin. Reconciling the dynamics of regional climate changes in the past requires an augmented understanding of hydrologic shifts, spatial and temporal distributions, and comparative analysis of the previous and current understanding of climatic fluctuations of the Great Basin. A more comprehensive understanding of playa stratigraphy and morphology will help to correlate climate and playa response.

Objectives for this study:

1. Determine procedures for the collection of GPR data in the study area
2. Compare GPR survey results with standard data collection methods
3. Describe the sedimentology of playa environments and associated physical processes observed at Silver Lake Playa
4. Assess the potential of GPR surveys to characterize the stratigraphy, sedimentology, and geomorphology

CHAPTER II

BACKGROUND

Playas

Playas, also known as dry lake beds, are ephemeral lakes. They are base-level plains in desert drainage basins, usually occupying the lowest area within their associated drainage basin (Goudie and Wells, 1995). Playas are commonly free of vegetation, almost perfectly horizontal, and contain fine-grained sediment deposits. Playas function as receptacles for water and sediments (Bowen and Johnson, 2012). Evidence strongly suggests that climate is the key controlling factor of playa development. The isolated circumstances under which playas form make them extremely useful analogs for understanding regional fluctuations in climate. Playas form within enclosed drainage basins as faulting, folding, and subsidence, driven by tectonic activity, blocks drainage.

Aeolian and alluvial deposition can also cause drainage blockage. Water recharge from ephemeral lakes and stream channels is crucial (Torgerson et al., 1986). Recharge occurs as stored water from ephemeral lakes and stream channels transmits through unsaturated zones to underlying water tables (Hills, 1940). Non-clastic sediments make their way into the playa system via groundwater. Fluvial and aeolian processes transport clastic sediments into the system. As fine-grained clastic and non-clastic deposits accumulate, the geomorphological consequence is a smooth, hard, almost impenetrable surface.

Playa-lunettes

Playa-lunettes get their name from the crescent moon shape (Hills, 1940) in which they generally occur. Lunettes are eolian dunes, varying in size from one to 150 meters in height, that tend to form along the leeward margin of playas through a combination of processes. Lacustrine, fluvial, and aeolian processes gather sediment from multiple sources within the playa system, producing a multimodal grain-size distribution (Cooke et al., 1993). These highly mixed sediments make interpretation very difficult and have been the cause of debate regarding the evolution of playa-lunettes.

Fan-deltas

As defined by Holmes (1965), fan-deltas are alluvial fans prograding directly into a standing body of water. Fan delta deposition generally occurs when there is a sufficient source of material for deposition located within proximity of the mouth of a high-relief drainage basin. Debris flows are the dominant process in fan delta formation. These formative debris flows tend to occur with high-intensity and low-periodicity (Roberts et al., 2003). Fan-deltas produce small-scale wedge-shaped sediment deposits, displaying highly varied current patterns and abrupt facies changes. The subaerial component is an alluvial fan comprising debris flow, braided channel, and sheet flood deposits (McPherson et al., 1987). The subaqueous component of a fan delta deposits into a standing body of water. Subaqueous components of fan-deltas are distinguishable from those related to alluvial fans and flood basin deposits by examining subaqueous debris-flow deposits that grade from the subaerial debris flow tongues of the fan-delta plain. As fan-delta debris flows prograde into standing water, fluidity increases, and debris flows devolve into more dilute density currents. Subaqueous debris flows interbed with subaerial debris flows and lacustrine flood basin deposits (Fig. 2). Reworking of the subaqueous component of fan-deltas also occurs and is dependent on wave energy, littoral currents, tidal flux, and tectonic setting (Gloppen and Steel,1981).

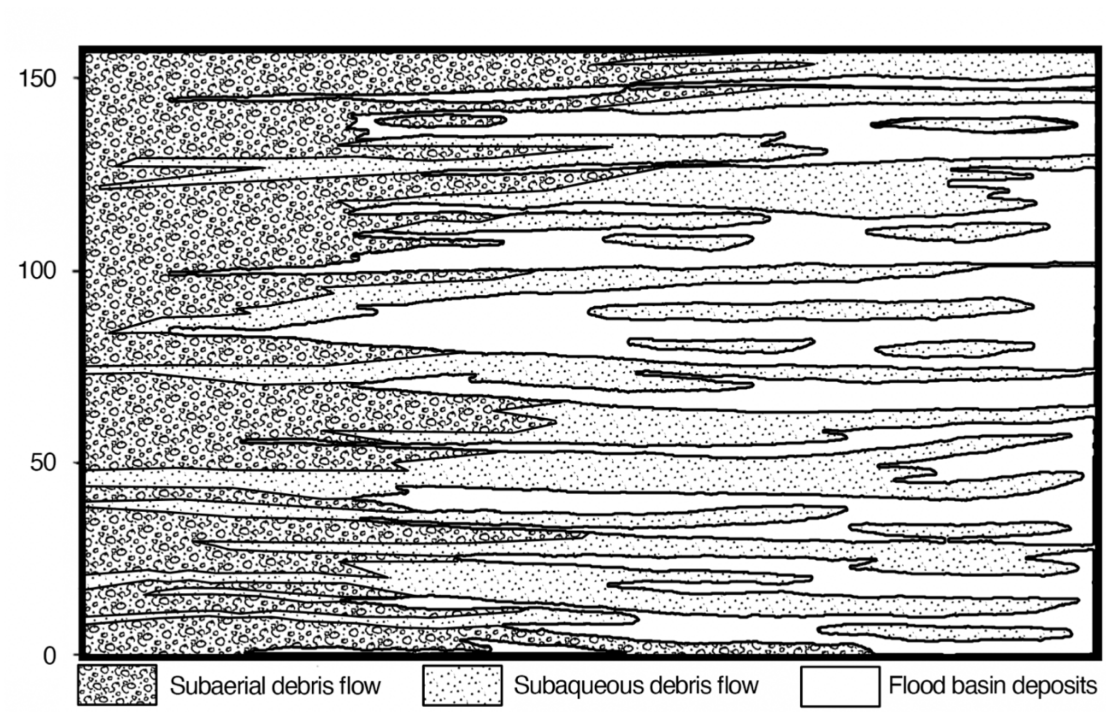

Figure 2. Stratigraphic relationship between subaerial and subaqueous debris flow deposits and lacustrine flood basin deposits (modified from Gloppen and Steele, 1981).

Ground Penetrating Radar

Ground-penetrating radar works by sending electromagnetic waves into the ground with an antenna-transmitter device, which can be monostatic (single-element for transmitting and receiving) or bistatic (separate transmitting and receiving elements), which are subsequently received by an antenna receiver device. This study uses ground-coupled shielded antenna devices (Ardekani, 2013). This type of GPR antenna device works as the operator places it into direct contact with the area of study or in close proximity to the work area's surface (Zajicova and Chaman, 2019).

Electromagnetic waves emitted and received by the GPR antenna reflect off boundaries possessing different electromagnetic properties. The strength of reflections is an effect of the contrasting relative dielectric permittivity (RDP) of buried features and bedding planes (Lanzarone et al., 2019). The resolution of data is dependent on the signal frequency (wavelength) and the size of the device's antenna used in the GPR study. GPR systems are usually composed of a modular system, allowing for the application of devices that produce higher or lower frequencies. Typically soil studies employ antennas working at 500 MHz or more. Higher frequency antennas allow for higher resolution in materials such as soil but are less capable of reaching the depth of lower frequency antennas (Zajicova and Chaman, 2019). Electromagnetic wave reflection facilitates the detection of layer boundaries (Van Dame et al., 2003). The relative strength of reflections is an effect of the contrasting relative dielectric permittivity (RDP) of buried features and bedding planes (Fig. 3) (Lanzarone et al., 2019).

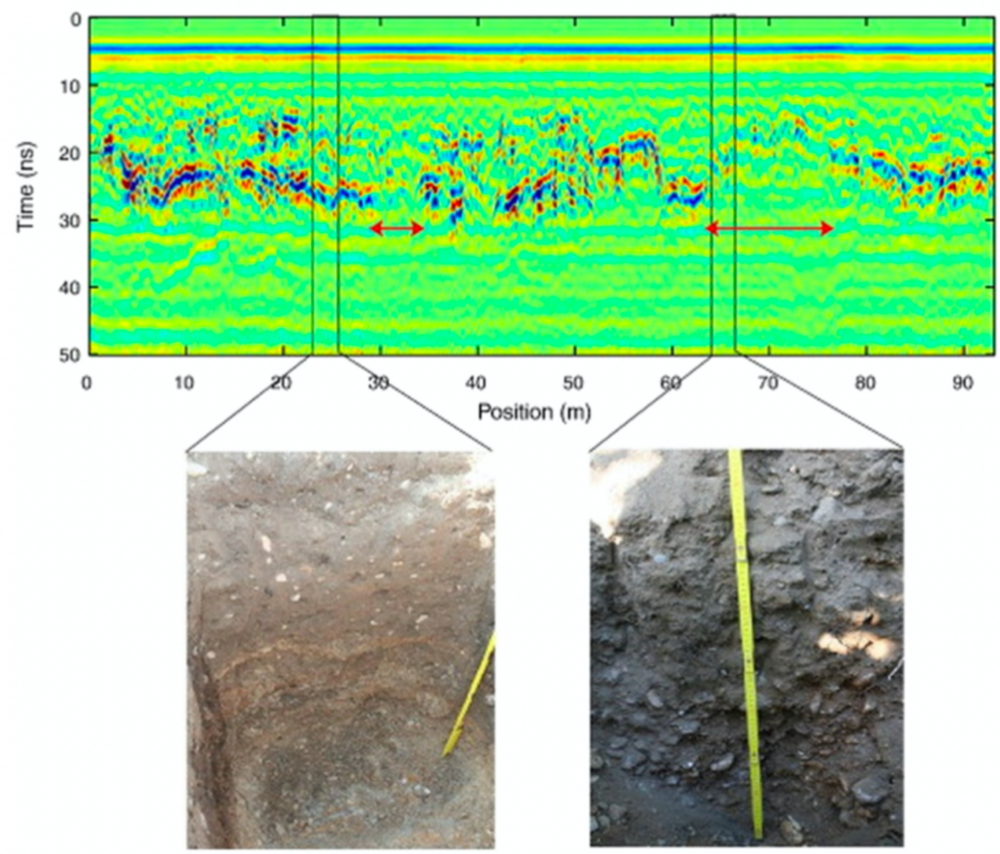

Figure 3. Example of a 2D radargram (top) illustrating the boundaries between layers of differing dielectric permittivity (RDP). Electromagnetic wave velocities measured in nanoseconds (ns) determine boundary depth (Time). The boundary between layers with differing RDP is visible in the zone between 20 and 30 ns, verified by soil profiles (bottom) (Lanzarone et al., 2019).

Ground-penetrating RADAR has applications in the detailed quantitative analyses of soil variability and composition. GPR shows advantages over other geophysical tools when working in shallow earthen strata (Doolittle et al.,1995). Accurate data interpretation requires the interpreter to know the survey's center frequency, usually within +/- 50MHz of the antenna frequency in Use (Adepelumi et al., 2013). Selecting the proper antenna frequency for the study area is critical to achieving well-resolved images. Higher frequency antennae produce high-resolution images in shallow soils of low conductivity, where low-frequency antennae can reach greater depths with the sacrifice of image resolution (Doolittle et al.,1995). Each survey requires a unique plan for data acquisition and interpretation (Zajicova et al., 2019). Soil conductivity is a crucial factor in the suitability of GPR application in an area of study. GPR is most effective in electronically resistive materials like sand, limestone, gravel, and peat. Also, soils saturated in freshwater react well. High salinity levels in the medium of saturation attenuate the EM signal, affecting the resolution and efficacy of using GPR (Bristow and Joi, 2003). Soil maps and classification systems can help assess if the Use of GPR is feasible in specific studies. As there are no previous studies of Silver Lake Playa available to aid in soil identification, application and selection of the appropriate antenna frequency was evaluated in situ.

Radar data from analysis of subsurface structures yield "radar facies." A radar facies is a mappable, three-dimensional sedimentary unit, visualized by radar reflections, exhibiting characteristic sedimentary properties, beneficial for interpretation and comparative analysis with other facies in a given profile (Roberts et al., 2003). Radar facies analysis can establish the depositional architecture components associated with debris-flow-dominant fan delta environments.

GPR Data Processing

Removal of noise via processing of GPR data sets results in a more readable radargram. Standard processing methods used on GPR survey data are velocity analysis, stacking, migration, and noise reduction (Chen et al., 2004). Bandpass filtering of data will remove frequency-specific noise in GPR data. Data collected by common midpoint can be processed using velocity analysis. Calculation of travel time considers antenna offset and velocities, producing a velocity profile for subsurface media. Stacking decreases the energy of noise while simultaneously increasing energy from reflected signals, improving the signal-to-noise ratio

CHAPTER 3

STUDY AREA

<u>The Great Basin</u>

The Great Basin of Western North America is over 500,000 km^2 and lies geographically across California, Oregon, Idaho, Utah, Arizona, and most of Nevada (Fig. 4). It is a vast collection of mountain ranges and basins with no external surface drainage (i.e., an endorheic basin). Ongoing regional uplift has created a high relief between mountain ranges and subsequent intermontane basins (Camilleri, 2013). Steep gradients deeply incise mountain fronts, producing alluvial fans that fringe mountain bases with lacustrine deposits and alluvium.

Figure 4. Map of the Great Basin of western North America (modified from Rand McNally, 1998).

Geology of the Great Basin

The late Precambrian (750 Ma) to Tertiary (65 Ma) bedrock of the Great Basin of Central Nevada contains a full spectrum of rock types. The area that is now the Great Basin was a continental margin fed by sedimentation from the western continental landscape to produce sedimentary rock. During the Paleozoic, sandstones, shales, and limestones formed in this marine sedimentary basin (Stewart, 1978). An active subduction zone developed as the continental margin evolved. Violent volcanic eruptions, produced as the area became an active subduction zone, led to ashflows, basaltic lavas, ignimbrites, tuffs, and rhyolite flows (Dickinson, 2006). The intrusion of igneous plutons served to metamorphose Paleozoic sedimentary rocks and created the region's before-mentioned volcanic activity (Kleinhampl et al., 1985). Low angle thrust faults cut the metamorphosed and folded Paleozoic rocks from west to east during the Antler and Sonoma orogenies. The modern topography of the region developed into what we see today as the Late Paleozoic compressional tectonic regime shifted to an extensional regime during the Miocene (Smith and Miller, 1990). As uplift occurred during the Cenozoic, rivers incised fault-bounded horsts, creating deeply dissected mountain uplands. Drainage from mountain ranges flowed into intermontane basins from east and west, primarily on bedrock.

The Owyhee Plateau

The Owyhee Plateau is an older block of less modified and isolated continental lithosphere (Hou et al., 2013) located immediately adjacent to the Great Basin endorheic basin and partially within the Great Basin section of the Basin and Range Province (Fig. 5). The Owyhee Plateau is an expanse of vast plains and deeply incised river valleys within isolated mountain ranges. The Owyhee Mountains are primarily granite, while the uplands are predominantly rhyolitic with welded tuffs, ash deposits, silica volcanic flows, and wind-blown loess (Hou et al., 2013). The northern portion of the Owyhee Plateau is generally an area of higher relief, where higher elevations see snow accumulation contributing to streamflow. The limited topographic relief in the southern part of the Owyhee Plateau, located in northern Nevada, has produced numerous small playas (i.e., surface area < 5 km^2) with generally homogenous watersheds. Some of these playas have well-developed playa lunettes. These small playas and playa lunettes have evolved in response to long-term climate patterns. However, they are susceptible to small-scale changes in climate, making them potentially important repositories of paleoenvironmental data for the region.

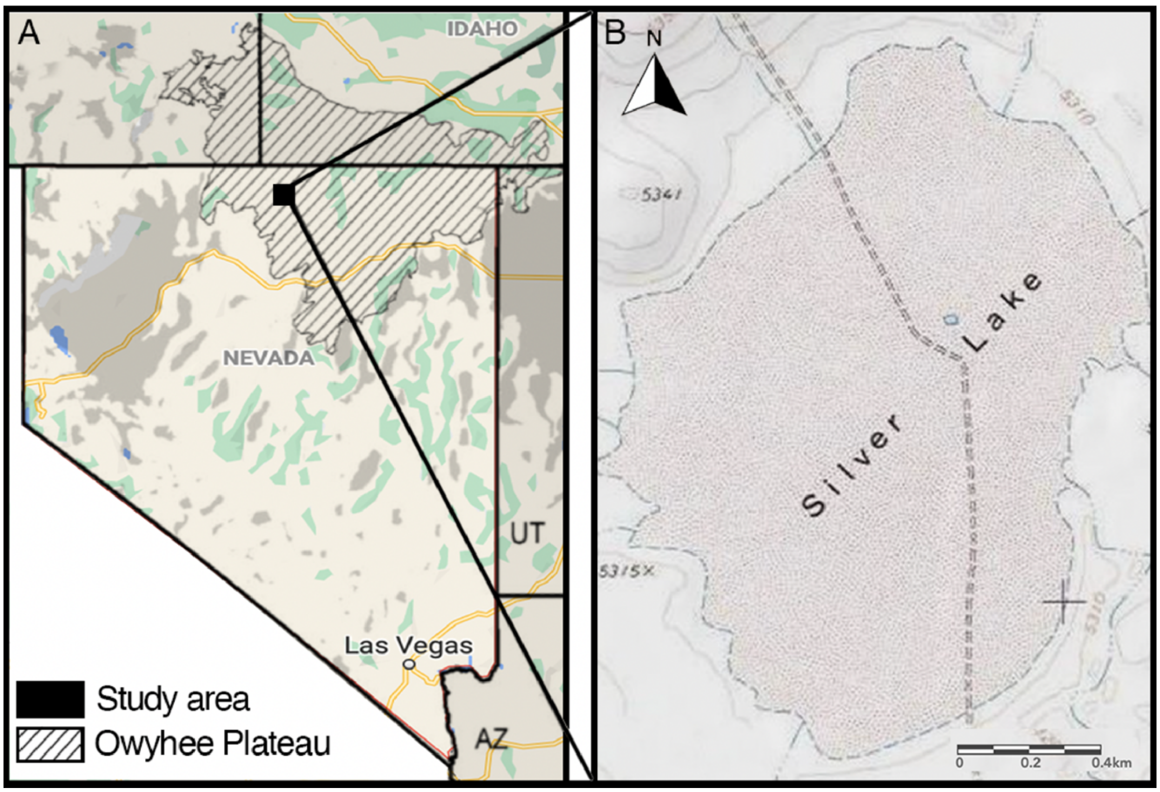

Figure 5. (A) Owyhee Plateau indicated by hatched polygon and research area indicated by a black box (modified from Collins, 2019). (B) Closer aerial view of the study area. The dashed line indicates silver Lake playa (modified from Google Earth).

Silver Lake Playa

The focus of this study is Silver Lake Playa, located in northern Nevada in the southern region of the Owyhee Plateau (Fig. 5B). Silver Lake Playa is the terminal playa in a "spill-and-fill" playa complex and a part of the entire Silver Lake Playa complex, including a cluster of six hydrologically connected playas within northern Nevada. The subsurface mapping of key features within Silver Lake Playa and its lunette could prove helpful in any future investigation of the morphology and stratigraphy of the entire Silver Lake Playa complex.

There are no studies on playas in the Owyhee Plateau of northern Nevada. This region presents us with a unique opportunity for insights into playa response to climatic fluctuations because of the geographically isolated nature of playa systems. As we examine the stratigraphy of Silver Lake playa, we hope to identify and characterize features that indicate regional climate for correlation within other systems in the Central Great Basin. We also hope to locate sites for future coring and trenching.

Areas of Interest

The focus of the GPR Survey is the delta on the northwest margin of the study area and the playa-lunette on the southwest margin (Fig. 6). After visual inspection of the study area, the dimensions and layout of the GPR surveys were determined, resulting in the best possible outcome for the study with the time and resources available. Initial test scans completed on-site determined the 350MHz antenna was best suited to scanning the playa's subsurface.

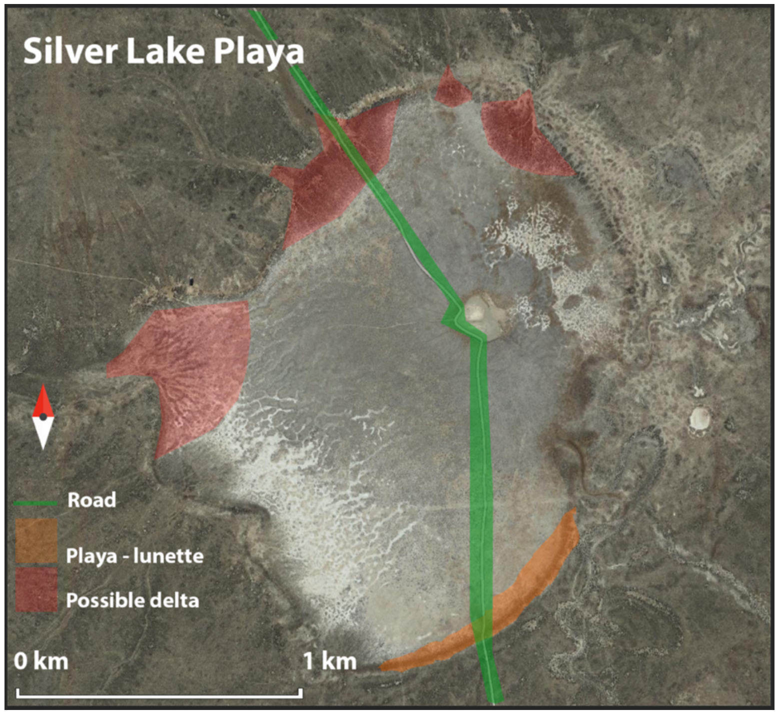

Figure 6. Aerial view of Silver Lake Playa. Deltas are in red. The playa lunette in the southwest margin of the playa is in orange (modified from Google Earth).

CHAPTER 4

METHODS

GPR Survey

This study employed the Use of a Geophysical Survey Systems, Inc, GPR unit, rented from the Department of Geosciences at the University of Tennessee, Knoxville (Fig. 7). The entire GPR package includes one 350 MHz antenna for deeper imaging while still maintaining a high level of resolution, one 900 MHz antenna for less penetrative imaging but resulting in a higher level of resolved images, one digital display, four lithium-ion batteries, and all necessary cables and chargers.

Figure 7. Pictured is a GSSI 4000 GPR control unit and all-terrain cart fitted with a 400MHz antenna overlooking auger hole A1.

Initial in situ inspection of soil in the study area presented as highly sandy, silty, and possibly containing clay. The typical range for the dielectric constant of sand is 3-5, and of clay is 5-40 (Table 1.). After determining the sediment's relative dielectric permittivity (RDP) in the study area, the 350 MHz antenna was deployed using a dielectric constant setting of eight on the GPR unit. The combination of a 350 MHz antenna and dielectric constant setting of eight appeared to yield the highest resolution data at an acceptable depth for this study.

Table 1) Common radar responses for materials during GPR data set collection (modified from Fisher et al., 1992).

MATERIAL	DIELECTRIC CONSTANT	VELOCITY m/ns
Air	1	0.30
Distilled Water	80	0.033
Fresh Water	80	0.033
Sea Water	80	0.01
Dry Sand	3 - 5	0.15
Saturated Sand	20 - 30	0.06
Limestone	4 - 8	0.12
Shale	5 - 15	0.09
Silts	5 - 30	0.07
Clays	5 - 40	0.06
Granite	4 - 6	0.13
Dry Salt	5 - 6	0.13
Ice	3 - 4	0.16

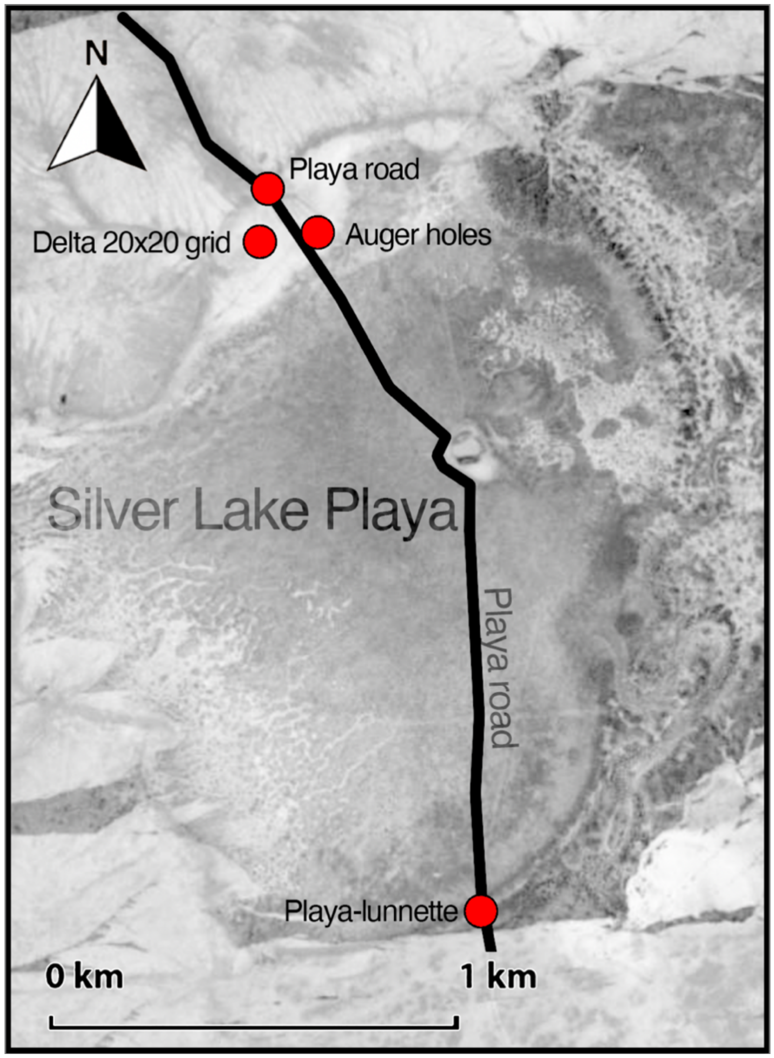

Figure 8. Location map of survey sites (indicated by red dot) within Silver Lake Playa (modified from USDA Farm Service Agency, 2021).

The acquisition design for Silver Lake playa entailed GPR dataset collection in four locations: a single radargram running along the playa road, five auger hole coring locations running parallel to the road, a 20x20m grid to the west of the road in the area of a possible delta, and the playa lunette at the southern margin (Fig. 8).

Playa Road Transect

The playa road was the first survey location (Fig. 8). This GPR survey took place directly on the upper section of the road, utilizing the roads' smooth graded surface free of debris to aid in data acquisition. The section of road surveyed is approximately 311 meters in length. The GPR survey was conducted using the 350 MHz antenna and an all-terrain cart. In-situ soil inspection indicated a dry silty to sandy soil type, and therefore a dielectric constant of eight was used. GPS data was collected for georeferencing the GPR data set with a Trimble R2 GNSS device.

Playa Road Auger Hole Sites

Simultaneous hand auger soil collection took place to the east, adjacent to the initial road survey (Fig. 8). After completing the road survey, GPR surveys were conducted at each auger hole location. An on-site inspection determined the use of the 350 MHz antenna and a dielectric constant of 8 for these GPR scans. There were five auger holes in total. These holes were georeferenced and assigned designations A1 through A5 from south to north. The total distance spanning A1 to A5 measures 185 m.

Delta 20 x 20-meter Grid

A 20x20 m section of the possible delta was selected for GPR data collection (Fig. 8). Field navigation was constrained using flag markers and measured at five-meter intervals. The start and stop point of each transect was marked and georeferenced with a Trimble R2 GNSS GPS device in conjunction with Trimble TerraFlex for iOS on a mobile device. GPR surveys collected five perpendicular transects, each 20 m long, at 5m intervals, in a south to north orientation, employing the 350 MHz antenna and dielectric constant of 8.

Lunette Road Transect

The final GPR survey location was the playa-lunette road on the southeast margin of Silver Lake Playa (Fig. 8). The GPR survey took advantage of the graded road that crosses over the playa-lunette in north to south orientation. The GPR survey on the lunette road was approximately 83 meters in length. The surface soil conditions were similar to that of the other locations surveyed within the playa and therefore deemed suitable for surveying with the 350 MHz antenna and a dielectric constant setting of 8.

Topographic Survey

GPS data was collected employing a Trimble R2 GNSS GPS device and Trimble TerraFlex for iOS. TerraFlex for iOS is a cloud-based data collection solution that allows for the collecting and uploading of data to an online server, where it can be pre-processed and accessed. The Trimble R2 GNSS device mounted to a 2-meter pole and the Trimble TerraFlex software collected GPS survey data for the playa road, auger hole coring sights, possible delta location 20x20 meter GPR survey, and the playa lunette.

Soil Collection

Collection of core samples in key locations (Fig. 8) of the study area for comparative analysis with radargrams in the examination of sediment stratigraphy was performed with a three 1/2-inch hand auger at 5 cm intervals to a depth of 1 meter. The sedimentary structure of each sample was unobservable due to the disruptive nature of the collection method. The presence of an impenetrable subsurface layer inhibited coring at depths of more than one meter. This impermeable layer was visible in the GPR radar data set for each auger hole location (Fig. 9). Soil samples were collected and stored in polypropylene bags marked with location and depth in preparation for transport back to

MTSU for analysis. A Trimble GNSS device collected GPS data for each auger hole extraction site at sub-meter accuracy. After extraction of soils, the GSSI GPR device, employing a 350Mhz antenna in an all-terrain cart, collected subsurface data for each collection site as a two-meter long transect bisecting each auger hole in a South to North orientation.

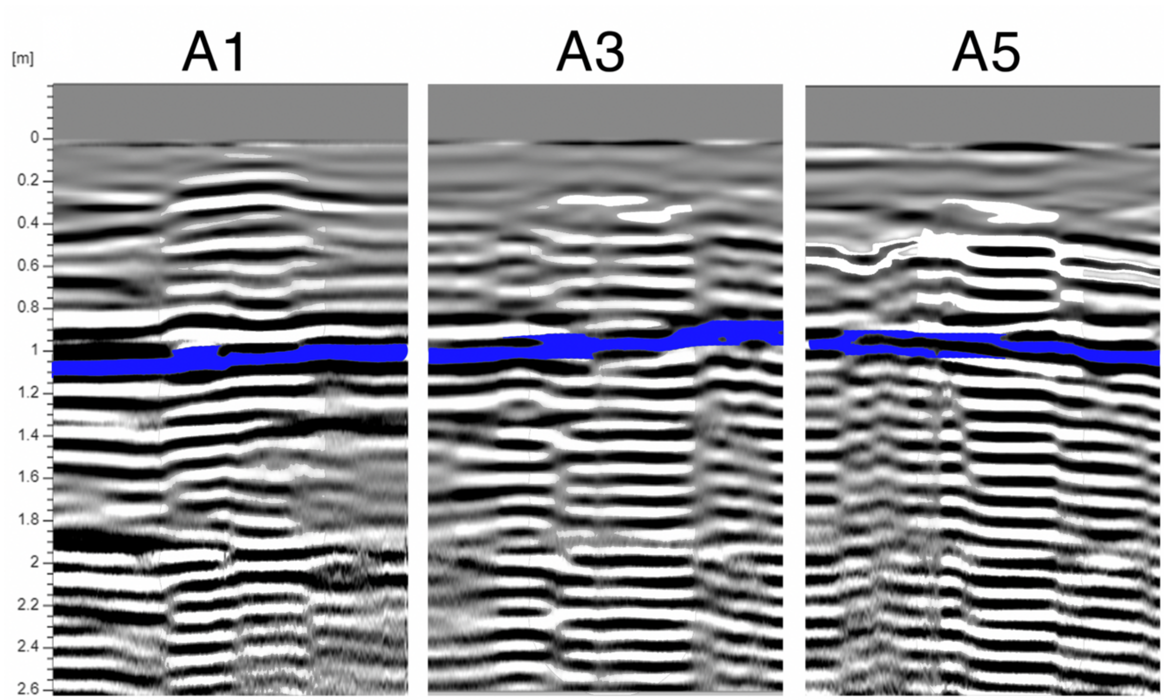

Figure 9. GPR profiles from auger holes A1, A3, and A5. Impermeable surface indicated in blue.

CHAPTER 5

RESULTS

GPR Processing

GPR survey data sets collected vary only slightly in resolution and quality. The attenuation of the signal in the shallowest depths of the radar profiles is most likely due to lithologies with little dielectric contrast (Lanzarone et al., 2019). Signal attenuation is evident at depths of 1.2 meters and greater.

All GPR data were processed using MALAVISION GPR processing software following standard best practices in GPR processing techniques (Cassidy, 2009). The first step of processing radargrams is the application of a DC offset to correct for signal saturation (Figs. 10 and 11). The airwave, groundwave, and near-surface reflections inject a large amount of energy into the collected radar signal. This considerable energy input saturates the signal, and the GPR receiver is unable to adjust between vertical stacks (Fisher et al., 1992). The result is a buildup of low-frequency "wow" on the high-frequency signal trace arrivals. This low energy "wow" has a masking effect on the signal traces. DC signal saturation is constant across the signal and can be filtered out with DC offset, unmasking the signal and allowing for better visualization. MALAVISION's proprietary software algorithm automatically sets this low-cut filter (Fig. 10).

Transmitted wavefields spread geometrically. Signal trace indicates the later arriving trace is attenuated in signal strength, presented as low-amplitude signal traces. After correcting for DC offset, an automatic gain control (AGC) corrects for the attenuation of data at depth (Figs. 10 and 11). A time-variant trace equalization or AGC can be applied to recover relative amplitude information, equalizing the attenuated signal and allowing better data visualization (Fisher et al., 1992).

After applying the AGC, a background removal filter helps improve the visualization of the data even further (Figs. 10 and 11). The background filter removes horizontal or near to horizontal features from data. The algorithm employed by MALAVISION applies a horizontal spatial high pass filter to the data, which has a similar output to running a subtract mean trace filter on the data. The remaining trace is actual data with this "background" data removed.

The hyperbola matching function within MALAVISION performed two-way travel time to depth conversion for all profiles. The selected average velocity constant for all profiles was 0.07 m/ns, typical for dry silty to sandy soils (Lanzarone et al., 2016).

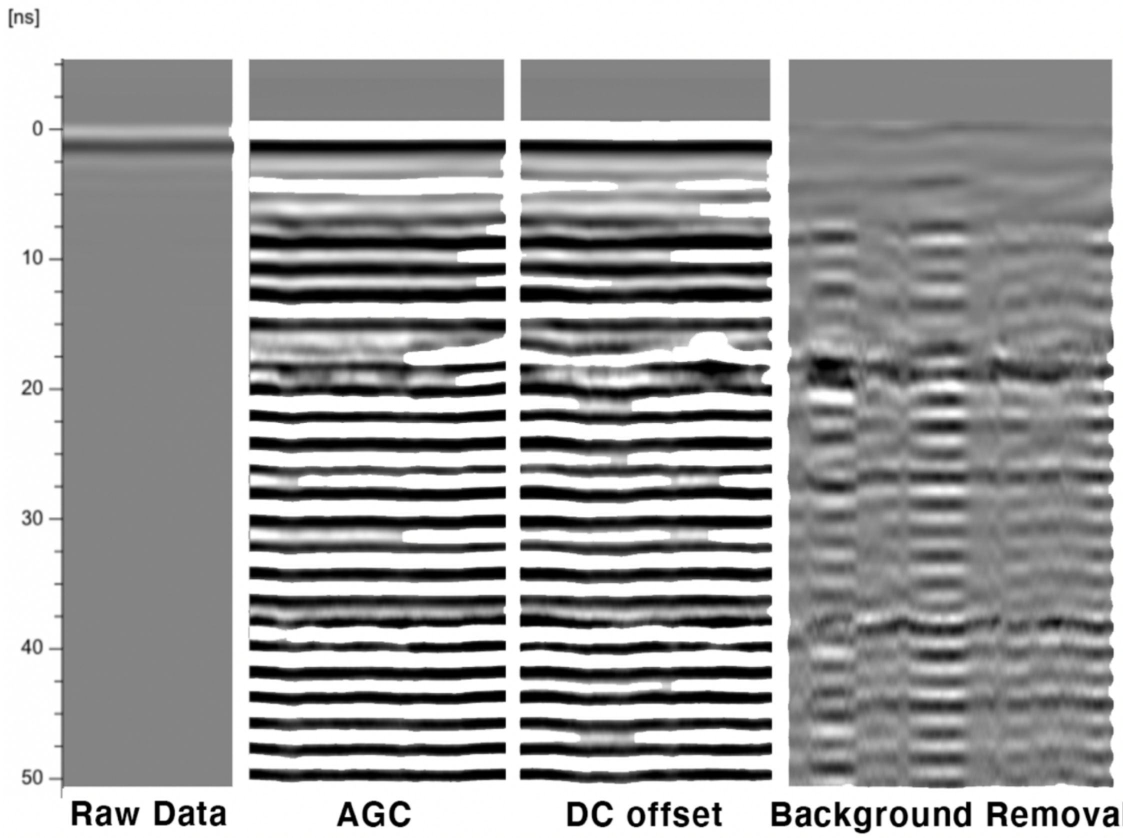

Figure 10. From left to right, raw data is uploaded into MALAVISION from the Delta road GPR dataset, where AGC, DC offset, and Background Removal filters are applied. The output is a very readable radargram.

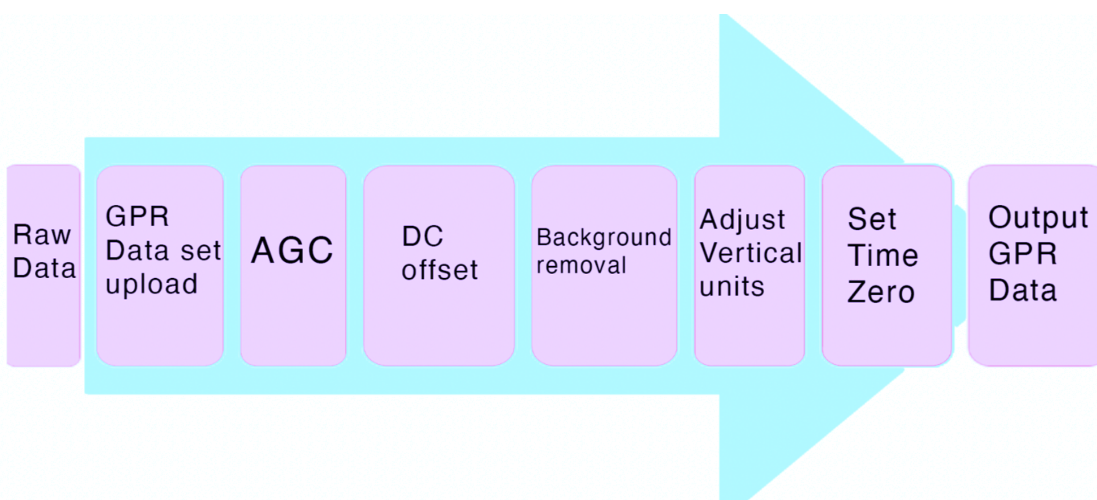

Figure 11. Flowchart of GPR data set processing.

Soil Sample Processing

Soil samples from auger holes A1, A3, and A5 were selected were selected for analysis. All organics were removed from samples by application of a solution of H_20_2 at 27 ^oC. After removing organics, a 5.5 g/L solution of hexametaphosphate deflocculated samples. Analysis of grain-size distributions (GSD) for each sample employed a Malvern Mastersizer 3000 laser diffraction particle-size analyzer equipped with a Hydro EV accessory (wet sample dispersion attachment). The Mastersizer performed an analysis of each sample in triplicate interspersed with a sampling of test dust (Powder Technology Inc.:ISO 12103-1, A4 Coarse Test Dust) to monitor the accuracy of testing.

Topographic Processing

GPS data collected with Trimble TerraFlex for iOS were downloaded into a CSV file from the Trimble cloud server. The raw XYZ coordinate data were pre-processed in Excel to eliminate any GPS data points not needed for the localized study. The CSV file was input into ESRI ARCMAP and point data for all research locations were integrated into a topographic base map to use in generating figures.

CHAPTER 6

DISCUSSION

GPR Profile Interpretation and Facies Identification

Post-processing GPR datasets enables the interpretation of visible reflection surfaces within the profiles. Varied lithologies appear in GPR radargrams as reflective surfaces. The strongest reflections in radargrams typically represent boundaries of distinct lithology. Less visible reflections tend to represent interbedded features within the subsurface, while areas of greater dielectric contrast present as stronger reflections.

Superimposed line drawings over GPR profiles aid in the interpretation of radargrams. Line drawings reinforce and enhance the actual radargram images (Table 2), making interpretation and identification of radar facies easier. During the interpretation of all data sets associated with this study, features of highest reflection were traced first, followed by areas with weaker dielectric contrast (after Lanzerone et al., 2019).

Table 2) Description and interpretation of radar facies observed in the Silver Lake Playa GPR dataset.

Description	Original Pattern	Interpretation
1 Mounded radar facies		
2 Low relief transgressive radar facies		
3 Concave radar facies	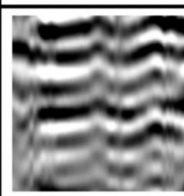	
4 Horizontal radar facies	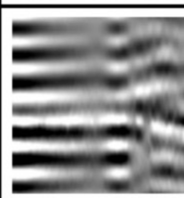	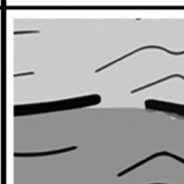

Facies Interpretation and Description for Silver Lake Playa

Mounded radar facies, Facies 1

Convex reflection patterns presenting in mounds or hummocks characterize this facies (Table 2). The mounded reflections in the data set can appear as isolated structures, stacked structures, or interfingered with other reflected surfaces (Fig. 14 PR5). Internal structures of mounds vary in appearance from intact to fragmented.

Interpretation, Facies 1

The similarity in visualized radar reflection surfaces investigated in other studies and identified in the facies of this study suggest that convex reflection surfaces represent the internal bedding and outer surface of debris flow lobes located in the subaerial portion of a fan delta (Roberts et al., 2003). Facies 1 could represent the main component of the topset beds associated with the fan delta. The visible convex nature and orientation of reflected surfaces characterizing Facies 1 are consistent with other observations of debris-flow deposits (Roberts et al., 2003). Modern debris flows deposit adjacent to previous deposits, creating an irregular to regular convex surface morphology. In several radar datasets, it is difficult to distinguish between possible point target reflections and hummocky structures occurring within proximity of each other. Roberts et al. (2003) made this same observation adding support to observations made in this study.

Low relief transgressive radar facies, Facies 2

Facies 2 presents a range of high-amplitude reflective surfaces to low-amplitude reflective surfaces (Lowe et al., 2013). Reflective surfaces in Facies 2 appear to undulate slightly (Table 2; Fig. 14). Thickness varies from 0.2-0.6m. Attenuation of GPR signal in Facies 2 could be due to the higher silt and clay content in soils.

Interpretation, Facies 2

Roberts et al. (2003) identifies reflections very similar in appearance to reflections observed in Facies 2 of this study as shoreface deposits of a fan delta. Wave reworking of the subaerial component of the delta, fluvial deposits, and the edge of the debris-flow lobes could have created this wide thin bed of sediment (Blair and McPherson, 2008; Roberts et al., 2003).

Concave radar facies, Facies 3

Facies 3 presents as alternating high to moderate contrast reflection surfaces with concave geometries (Table 2; Fig. 14). The extent of these concave surfaces is limited, but the continuity is strong where they occur. These concave geometries carry through highly reflective possible bounding surfaces in the datasets.

Interpretation, Facies 3

The continuous concave reflection surface visualized in the radar data set denotes the possible location of distributary channels in the fan delta. Typical distributary channel boundaries appear in GPR datasets as well-defined concave reflective surfaces (Roberts et al., 2003), congruent with data visualized in the Silver Lake Playa GPR data.

Horizontal radar facies, Facies 4

Facies 4 presents high-amplitude, parallel, and continuous reflection surfaces in the dataset (Table 2). There are slight lateral variances in contrast, but these strong reflective surfaces generally extend over a considerable distance.

Interpretation of Facies 4

Ground proofing with auger hole data from holes A1 through A5 (Fig. 13) correlates these high-amplitude reflective surfaces with a hard impermeable layer, consistent with the characteristics of typical playa surfaces (Goudie and Wells, 1995).

GPR profile interpretation

Playa road GPR dataset

Profile selection is a result of visual inspection of subsurface features and their apparent relevance to this study (Fig. 12). Figure 13 shows profiles from the "Playa road" data set at distances of 15m, 115m, 150m, 230m, and 265m from the start of data collection. Each profile is five meters long and reads to a depth of 2.25 meters.

PR1

Profile PR1 (Fig. 14) was taken at 15m into the principle transect. The top portion of profile PR1 shows low-amplitude reflections. Low-amplitude reflections in the upper section along all profiles in this dataset are likely due to the silt loam soil to silty soils found in the survey area (Fig. 16). These top layers of soil show little contrast in their dielectric contents. At 0.4 meters, there is a more reflective surface. Ground proofing made possible by soil and grain size analysis from hand auger coring at A1 (Fig. 16) shows a jump in sand content at that depth. The presence of sand would be consistent with the appearance of a higher intensity reflection at that depth (Lowe et al., 2013).

PR2

Between 0.4 meters and 0.8 meters, there is an increase in contrast of reflections. This increase in the amplitude of reflections could result from the concentration of more reflective sand during periods of deflation in the study area (Bristow et al., 2003). An increase in the amplitude of reflections at a depth of 0.4 to 0.8 meters is consistent across all profiles taken from the "Playa road" dataset for detailed examination. Low-amplitude reflective surfaces (Facies 2) dominate PR1, with one significant high-amplitude reflective surface (Facies 4), for which the most likely interpretation is a former playa surface.

PR3

Undulating and mounded medium to high-amplitude reflections (Facies 1,2,3) dominate Profiles PR2 and PR3 (Fig. 14). It is difficult to differentiate between possible hyperbolas caused by large point targets and mounded reflective surfaces (Roberts et al., 2003). The appearance of both together could indicate the interfingering of subaerial and subaqueous debris flow deposits and lacustrine flood basin deposits, as described by Gloppen and Steel (1981).

PR4

Profile PR4 contains examples of Facies 1, 2, and 4. There are three high-amplitude reflective surfaces, one at 0.2 meters, another at 0.8 meters, and a third at 1.6 meters. Low-amplitude reflective surfaces (Facies 2) appear truncated by overlying high-amplitude bounding surfaces suggesting wave reworking of the interface between subaerial and subaqueous zones, consistent with observed fan delta environments (Roberts et al., 2003). The very slightly undulating sub-horizontal reflections might also indicate the beach zone of the delta.

PR5

The three high-amplitude reflection surfaces from PR4 continue through to PR5, with only the third and lowest surface shifting in depth from 1.6 meters to 1.8 meters. PR5 shifts from Facies 1,2,4 to Facies 1,3,4, similar to observations made of PR3. Reflective surfaces observed in PR4 exhibit higher contrast and amplitude when compared to those in PR3, which could indicate a shift from silt-dominated soils to more silt loam soil, based on comparative analysis between soil samples and radargrams performed on auger holes A1 through A5. The presence of many mounded and concave surfaces would suggest the presence of debris flow lobes and channelized debris flows, placing this location on the subaerial delta plain (Roberts et al., 2003).

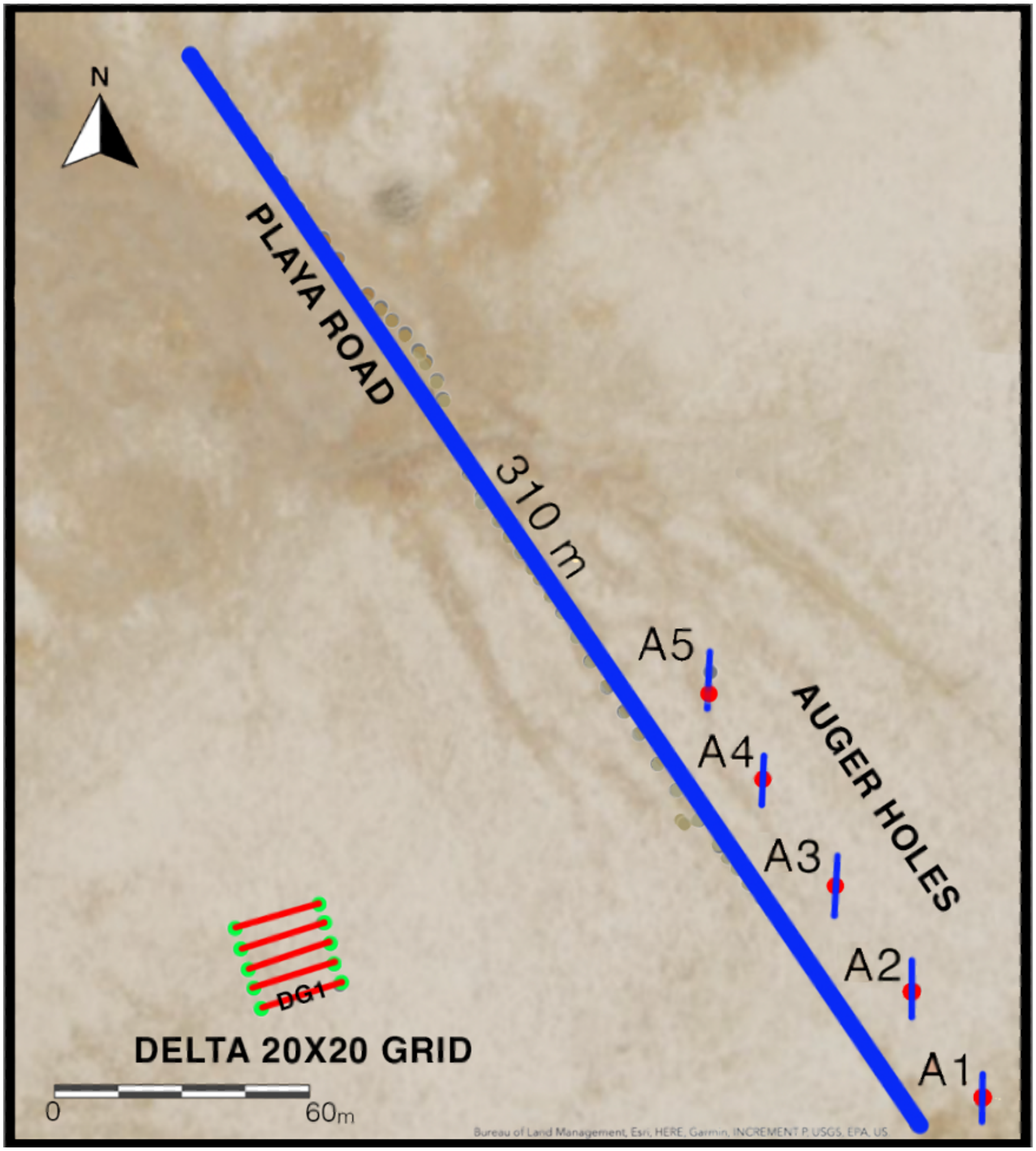

Figure 12. Map of "Playa Road" data set indicated by a blue line. The transect is 310 meters in length. The exact locations of Auger holes beside the road survey are indicated by red markers and labeled accordingly. GPR survey of each auger hole indicated with a blue line. The Delta 20 x 20 grid survey location is east of the playa road. Each transect's start and stop point is marked in green, and profile DQ1 is labeled. East to west running transects are indicated by red lines (modified from Bureau of Land Management, 2021).

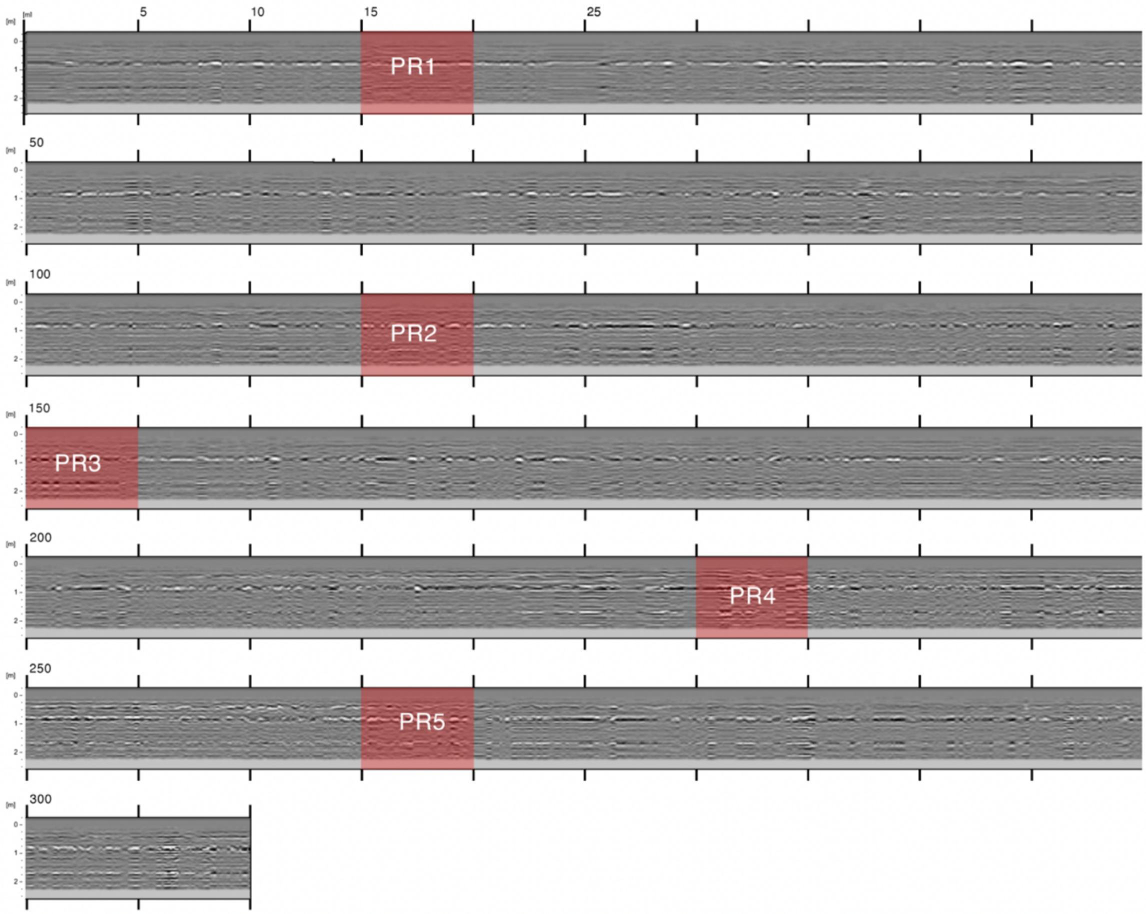

Figure 13. "Playa Road" data set in its entirety. Specific profiles from the data set (indicated in red) labeled PR1-PR5 were selected for interpretation (see Fig. 14).

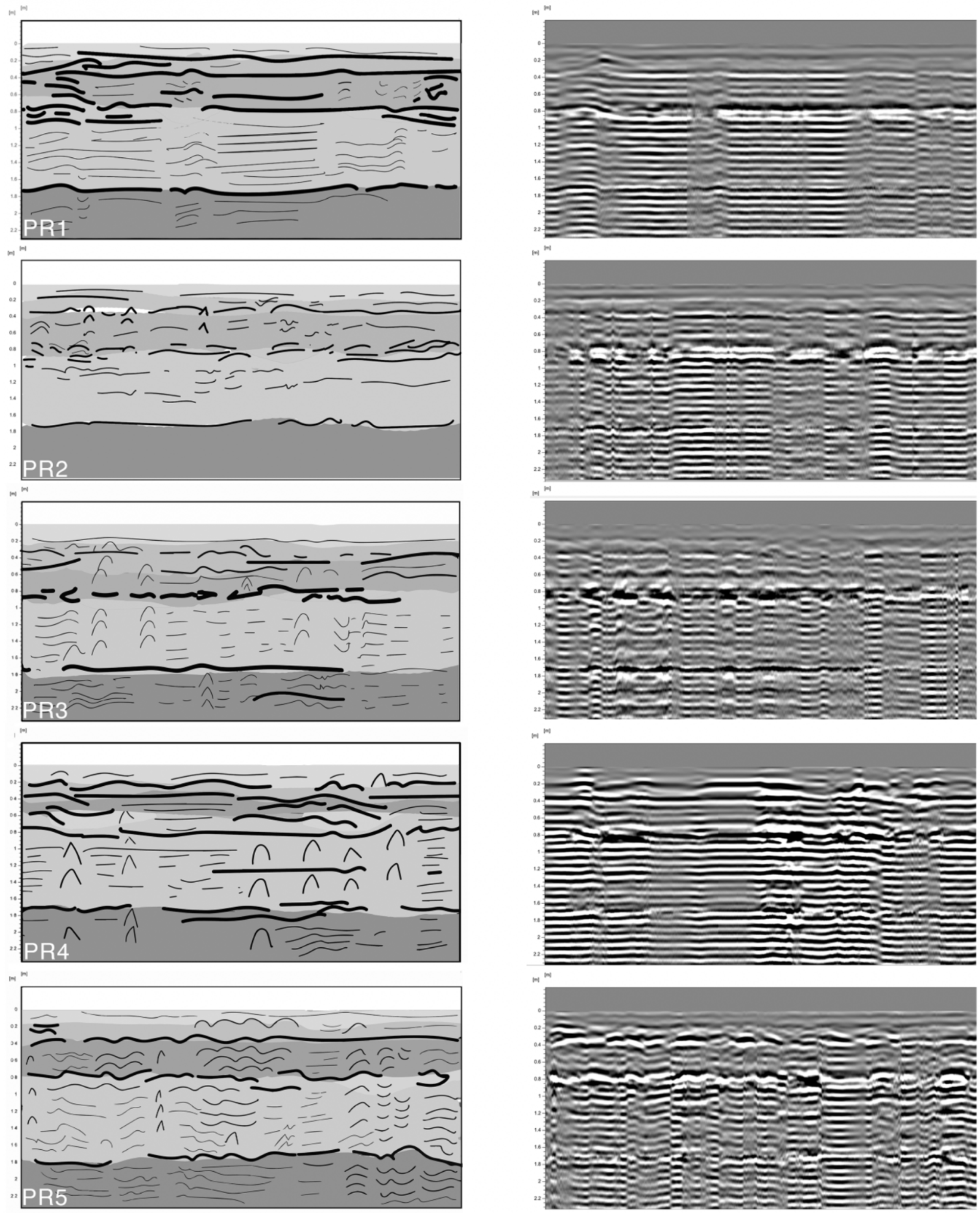

Figure 14. Silver Lake Playa "Playa Road" dataset at 15m (PR1), 115m (PR2), 150m (PR3), 230m (PR4), and 265m (PR5).

Auger hole GPR dataset

The purpose of collecting sediment samples and GPR profiles from this location was to facilitate ground proofing of the study area to aid in the interpretation of GPR profiles from datasets elsewhere in Silver Lake Playa. A comprehensive interpretation of auger hole datasets is not possible due to the disruption of subsurface features during coring. The hand auger apparatus was unable to collect samples past a depth of 65 cm due to an impenetrable surface present at each location. GSD for auger holes A1, A3, and A5 was determined using a Malvern Mastersizer 3000 and Hydro Ev attachment (wet sample dispersion unit) for comparative analysis against GPR profiles collected at the time of coring (Fig. 16). Overall, the GSD of A1 shows a fining-downward trend. There is an increase in sand-sized sediment from samples taken from 12-25 cm. The GPR profile of A1 shows a layer of increased amplitude at the same depth, which could indicate that layers of higher reflectivity in this and other profiles from the study area contain higher concentrations of sandy soils (Fig. 15). GSD analysis of holes A3 and A5 show relatively homogenous silty soils present from top to the bottom of the sample set. Visible in the GSD histogram are regular increases in sand concentrations that would appear to correlate to changes in amplitude of the GPR profiles for all holes. An overlay of samples higher in sand content on the GPR radargram at correlating depths shows high-amplitude reflections closely align with a higher sand content of samples (Fig. 15).

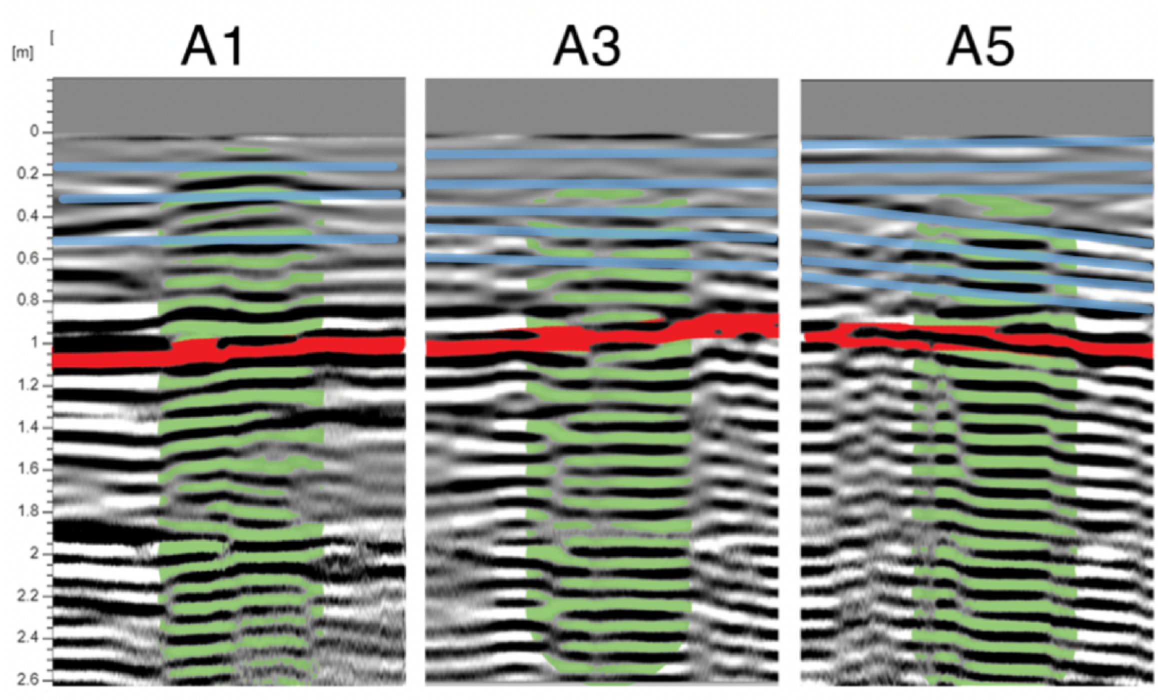

Figure 15. GPR radargrams of auger holes A1, A3, and A5. Green indicates soil disrupted by coring. Soils closer to the surface for auger hole A1 exhibit high-amplitude reflective surfaces. This increased resolution is most likely the result of the higher sand content of these soils and their distinct dielectric permittivity (Lowe et al., 2013). GSD of A3 and A5 show higher silt content, but an overlay of soils with higher sand concentration (shown in blue) at their recorded depths correlate with the high-amplitude surfaces in the GPR profiles. All radargrams show a distinct boundary at approximately one meter, likely the original playa surface overlain by alluvial deposits. Auger holes are visible as a break in the horizontal reflection lines in radargrams.

Figure 16. GSD for the three auger holes was performed with a Malvern Mastersizer 3000 and Hydro Ev attachment (wet sample dispersion unit). The raw grain-size data was brought into Excel and visualized in histograms showing sand (blue), silt (orange), and clay (gray) content at depth. Data for A3 and A5 show a more homogenous soil structure with only subtle variation. A1 shows a coarsening upward trend occurring at this location over time which could indicate deflation.

Delta 20 x 20 grid dataset (DQ1)

The GPR survey of the "Delta 20x20 grid" study area produced five 20m long GPR profiles. After processing and inspection of all radargrams from this dataset, it was determined feasible to interpret the southernmost profile (DQ1) alone, due to the similarity between all profiles in the dataset.

The most prevalent facies throughout DQ1 is Facies 1. Mounded reflective surfaces dominate the top bed of DQ1 (Table 2; Fig. 17). These stacked and overlapping mounded convex features could indicate debris flow lobes in the subaerial portion of a fan delta. Possible intermixed hyperbola in the profile could indicate wave reworking of previously deposited debris or large stones rafted by channelized debris flows (Roberts et al., 2003). Below the mounded surfaces, the profile shifts to low relief transgressive radar facies (Facies 2), interpreted to be the wave reworked interface between the subaerial and subaqueous portions of the delta. The presence of these features in DQ1 is consistent with features observed in PR3 and PR5 from the "Playa Road" dataset (Fig. 13). The Facies 4 type horizontal high-amplitude reflective surfaces seen in the "Auger hole" dataset and "Playa road" datasets are present in DQ1 at the same depths of one and two meters but lack contrast and appear segmented in the radargram. Salt intrusion via capillary action could explain the lack of contrast in these boundaries and indicate a source of direct groundwater discharge (Hills, 1940).

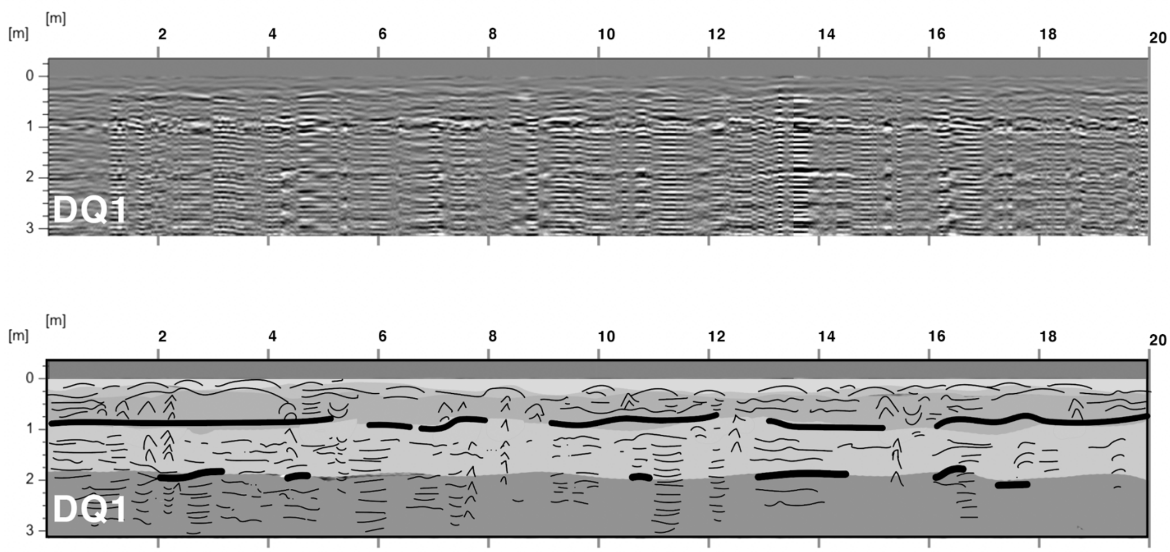

Figure 17. DQ1 is the southernmost GPR profile (top) from the Delta 20x20 grid location. The line drawing of DQ1's interpretation is below the original processed radargram.

Playa-lunette GPR dataset

The playa-lunette GPR survey collected one 82 meter long dataset utilizing the road which crosses over the central part of the playa-lunette. The GPR profile begins at the base of the windward side of the lunette, which faces the playa, travels south over the active crest of the lunette located midway through the transect, and extends another 40 meters onto the leeward side (Fig. 18). After processing and inspecting the data collected, one section of the profile was selected from five meters into the survey (LR1) and a second section from 40 meters into the survey (LR2). Ground proofing was not conducted on the lunette due to time limitations; therefore, the interpretation of data is theoretical.

LR1

Profile LR1 is located 5 meters from the base of the windward side of the lunette and appears to be dominated by Facies 1 high-amplitude mounded reflective surfaces (Fig. 20). High dielectric contrast in the GPR data in LR1 could indicate higher concentrations of sand. Twidale and Campbell (2005) characterize lunettes as being comprised of fine-grain silts. High sand content in lunette soils would be inconsistent with typical lunette morphology (Twidale, 2015). Facies 1 in this profile could indicate reworking of sediments or deposition by wave action during wet periods in the study area (Bowler, 1970). The profile is characterized by Facies 1 from five to approximately 15 meters, where high-amplitude reflections dissipate, and the profile appears to be dominated by low-amplitude horizontal reflective surfaces until another section of Facies 1-type mounded radar reflections appear at 25 meters and continues for another 10 meters. These repeated facies shifts on the windward side of the playa-lunette could indicate climatic shifts or wet-and-dry periods in the playa basin.

LR2

Profile LR2 is located 40 meters into the playa-lunette transect just past the active crest on the leeward side of the lunette (Fig. 19). Low-amplitude horizontal reflective surfaces characterize LR2 from the surface of the profile to a depth of three meters (Fig. 20). In correlation with ground proofing conducted in auger holes A1-A5, it would appear that soils in LR2 are predominately silty. No other identifiable radar signatures in LR2 correlate with facies observed in other parts of the study area. It is very likely that the possibly silt-rich sediments on the leeward side of the lunette are of aeolian origin, brought to their location through deflation of sediments from the playa surface (Thomas et al., 1993).

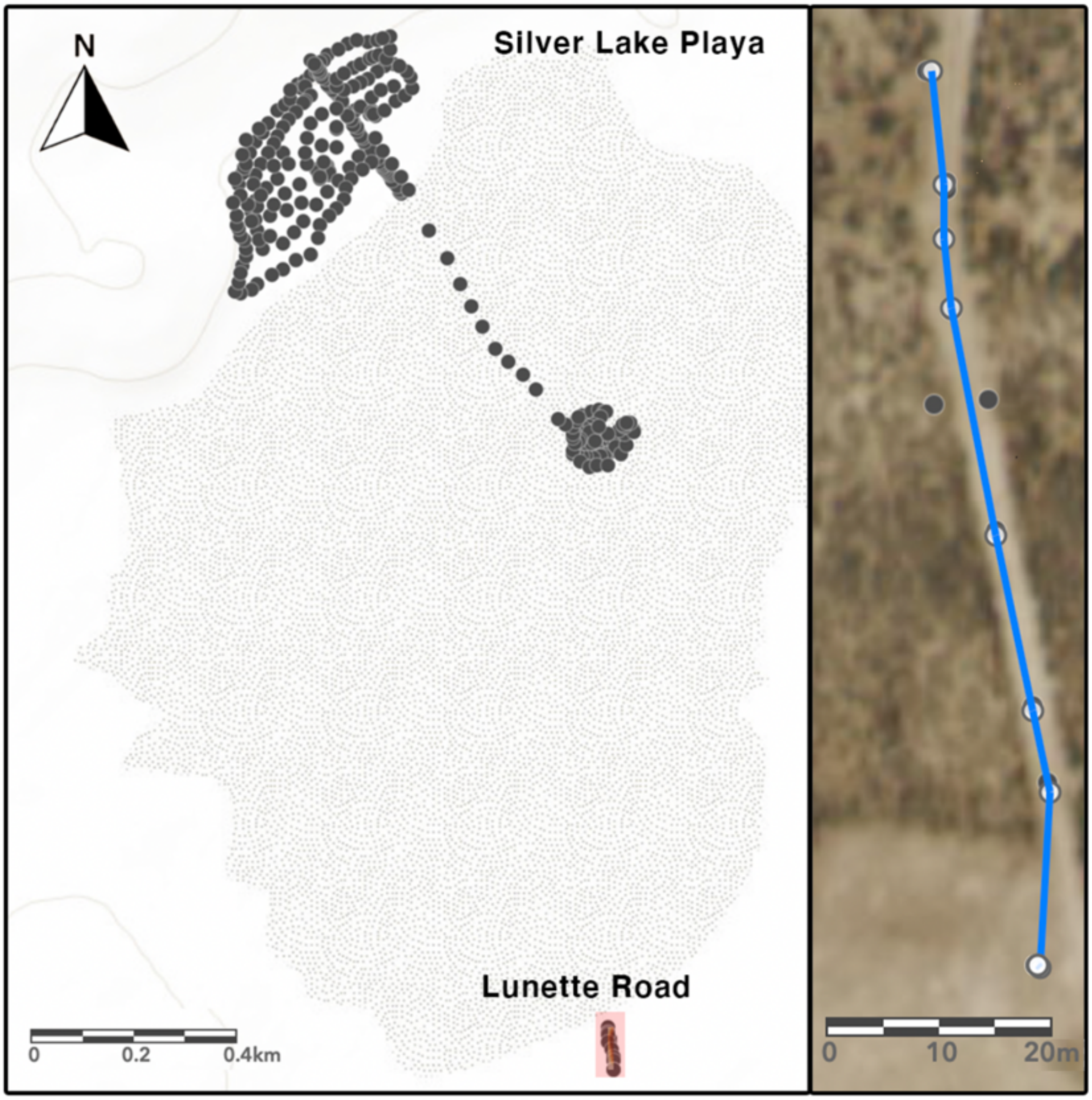

Figure 18. Map of the entire Silver Lake Playa study area (left) with the "Playa-lunette" GPR dataset in red and expanded (right). GPS data was collected, marking the path of the GPR survey of the playa-lunette from north to south (modified from Google Earth, 2022).

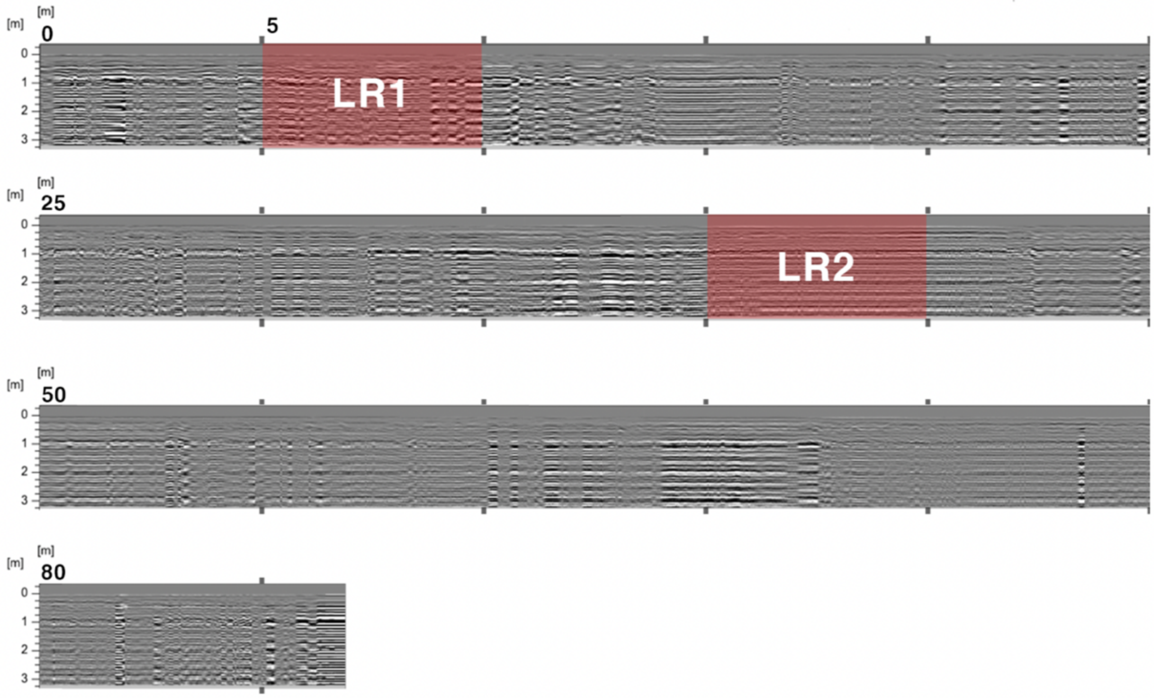

Figure 19. Playa lunette road profile from north to south measuring 82 meters in length. Profile LR1 is located at 5 meters, and profile LR2 is located at 40 meters (in red).

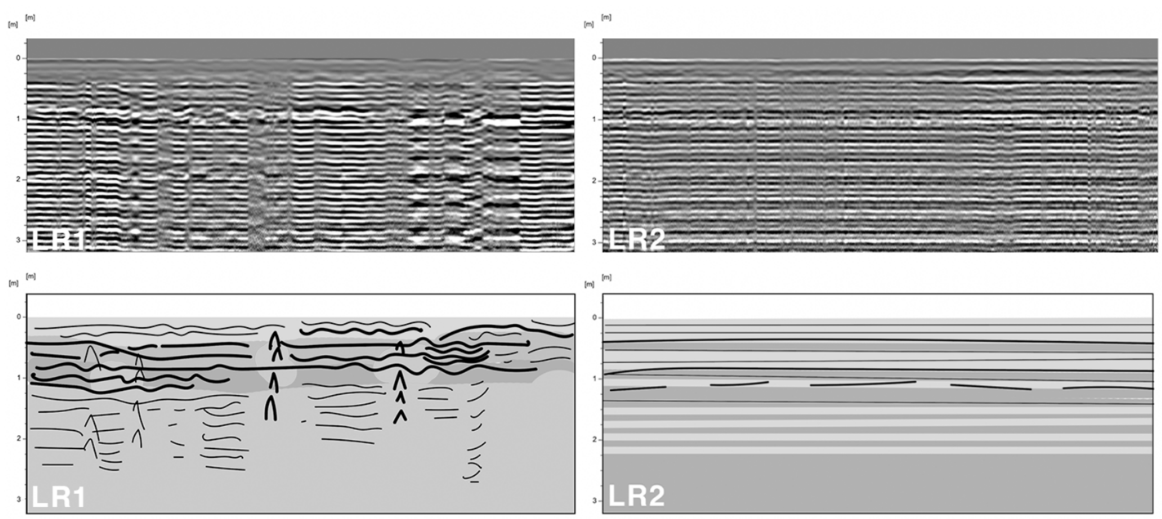

Figure 20. Raw GPR profiles for the "Playa-lunette road" GPR dataset (top) and line drawing interpretations (bottom) for Profiles LR1 at five meters and LR2 at 40 meters. LR1 represents the windward slope on the playa side of the lunette, and LR2 represents the point just past the crest of the lunette on the leeward side

CHAPTER 7

Conclusions and recommendations

GPR surveys captured radar data within Silver Lake Playa with sufficient resolution to distinguish recognizable reflective structures in the subsurface of each location. Results from all GPR surveys across the entire study area show a remarkable level of definition. The ability to differentiate between sediments of only slightly varied sand content seen in the ground proofing performed on auger holes A1, A2, and A3, is promising. More extensive ground proofing would aid in confirming the data are accurate.

To summarize, this study intended to discover if GPR is a viable data acquisition method for Use in semi-arid ephemeral environments, specifically playas. Efficacy may vary due to saltwater intrusion (Lanzarone et al., 2019). It is possible some masking of radar signal did occur in the Delta 20x20 grid dataset due to saltwater intrusion. Ground proofing was not conducted in this location due to time limitations, making suspicions of saltwater intrusion theoretical.

The MALAVISION Software suite proved to be a powerful tool in cleaning up datasets. The filtering performed by the Malavision algorithms pulled out very usable data when the raw profiles showed little promise. The proprietary Background Removal algorithm and AGC employed by MALAVISION were far more effective than their equivalent found in the Radan7 software package. Using advanced processing software in conjunction with new high dynamic range (HDR) GPR units manufactured by companies like MALA, GPR data collection in Silver Lake playa could be even more efficacious.

BIBLIOGRAPHY

Adepelumi, A.A., Faye, O., Akindulureni, J. (2013). Geophysical mapping of subsurface stratigraphy beneath a riverbed using ground-penetrating radar: Lagos Nigeria case study. *Universal Journal of Geoscience, 1*(1), 10-19.

Ardekani, M. R. (2013). Off- and on-ground GPR techniques for field-scale soil moisture mapping. *Geoderma, 200-201*, 55-66. doi:10.1016/j.geoderma.2013.02.010

Bird, B. W., Kirby, M. E., Howat, I. M., & Tulaczyk, S. (2010). Geophysical evidence for Holocene Lake-level change in Southern California (dry lake). *Boreas, 39*(1), 131-144. doi:10.1111/j.1502-3885.2009.00114.x

Blair, T.C., and McPherson, J.G. (2008). Quaternary sedimentology of the Rose Creek Fan Delta, Walker Lake, Nevada, USA, and implications to fan-delta facies models. *Sedimentology, 55*(3), 579-615. doi:10.1111/j.1365-3091.2007.00913.x

Bowen, M. W., & Johnson, W. C. (2011). Late Quaternary environmental reconstructions of Playa-lunette system evolution on the Central High Plains of Kansas, United States. *Geological Society of America Bulletin, 124*(1-2), 146-161. doi:10.1130/b30382.1

Bowler, J.M. (1970). Lunettes, in Late Quaternary environments: A study of lakes and associated sediments in southeastern Australia [Doctoral dissertation, the Australian National University]. PQDT Open. https://www.proquest.com/openview/a05cc2bb2d5165fedf606218d342f854/1?pq-origsite=gscholar&cbl=2026366&diss=y

Bristow, C. S., & Jol, H. M. (2003). An introduction to ground penetrating radar (GPR) in sediments. *Geological Society, London, Special Publications, 211*(1), 1-7. doi:10.1144/gsl.sp.2001.211.01.01

Camilleri, P. (2013). Geologic map and structure of the west-central part of the Grant Range, Nye County, Nevada. *The Geological Society of America Digital Map and Chart Series,14*(1), 1-25. doi:10.1130/2013.dmch014

Fisher, E., McMechan, G. A., & Annan, A. P. (1992). Acquisition and processing of wide-aperture ground-penetrating radar data. *GEOPHYSICS, 57*(3), 495-504. doi:10.1190/1.1443265

Chen, B., Hu, Z., Li, W. (2004, June). The utilization of GPR data in GIS. Proceedings 12th int. Conf. on Geoinformatics - Geospatial Information Research: Bridging the Pacific and Atlantic, 2004. Sweden: University of Gavle.

Cohen, A.S., Palacios-Fest, M.R., Negrini, R.M., Wigand, P.E., & Erbes, D.B. (2000). A paleoclimate record for the past 250,000 years from Summer Lake, Oregon, USA: II. Sedimentology, paleontology and geochemistry. *Journal of Paleolimnology, 24*, 151-182.

Collins, J., D. (2019). Late Quaternary paleohydrology and paleoclimate records of Silver Lake play complex on the Owyhee Plateau, Northern Nevada, Great Basin: Proposal to the National Science Foundation, Typescript.

Cooke, R.U., Goudie, A., and Warren, A. (1993). Desert geomorphology.London: UCL Press.

Dickinson, W. R. (2006). Geotectonic evolution of the Great Basin. *Geosphere, 2*(7), 353. doi:10.1130/ges00054.1

Doolittle, J. A., & Collins, M. E. (1995). Use of soil information to determine application of ground penetrating radar. *Journal of Applied Geophysics, 33*(1-3), 101-108. doi:10.1016/0926-9851(95)90033-0

Fisher, E., McMechan, G. A., & Annan, A. P. (1992). Acquisition and processing of wide-aperture ground-penetrating radar data. *GEOPHYSICS, 57*(3), 495-504. doi:10.1190/1.1443265

Gloppen, T. G., & Steel, R. J. (1981). The deposits, internal structure and geometry in six alluvial fan–fan delta bodies (devonian-norway)–a study in the significance of bedding sequence in conglomerates. *Recent and Ancient Nonmarine Depositional Environments,* 49-69. doi:10.2110/pec.81.31.0049

Goudie, A., & Wells, G. (1995). The nature, distribution and formation of pans in arid zones. *Earth-Science Reviews,38*(1), 1-69. doi:10.1016/0012-8252(94)00066-6

Google. (n.d. -a). [Google Map of silver lake playa, NV]. Retrieved September 15, 2020, from https://www.google.com/maps/@35.8368978,-86.4452608,14z

Edwin S. Hills D.Sc. (1940). The lunette, a new land form of aeolian origin, *Australian Geographer, 3*(7), 15-21, DOI: 10.1080/00049184008702196

Read, H. (1966). Principles of physical geology by Arthur Holmes. second edition. pp. XV + 1288. Thomas Nelson & Sons, Edinburgh. 1965. 84s. *Endeavour, 25*(95), 113. doi:10.1016/0160-9327(66)90095-0

Hou, T., Chen, C., James, D. E., Fouch, M. J. (2013). The instracrustal structure beneath the Owyhee Plateau, Oregon, from receiver function analysis. *Proceedings from the American Geophysical Union*, 4-31.

Kleinhampl, F.J., and Ziony, J.I. (1985). Geology of northern Nye County, Nevada: Nevada Bureau of Mines and Geology, Bulletin 99A, 172.

Lanzarone, P., Seidel, M., Brandt, S., Garrison, E., & Fisher, E. C. (2019). Ground-penetrating radar and electrical resistivity tomography reveal a deep stratigraphic sequence at Mochena Borago Rockshelter, southwestern Ethiopia. *Journal of Archaeological Science: Reports, 26*, 101915. doi:10.1016/j.jasrep.2019.101915

McPherson, J. G., Shanmugam, G., & Moiola, R. J. (1987). Fan-Deltas and braid deltas: Varieties of coarse-grained deltas. *Geological Society of America Bulletin, 99*(3), 331. doi:10.1130/0016-7606(1987)992.0.co;2

Munroe, J. S., & Laabs, B. J. (2012). Temporal correspondence between Pluvial Lake highstands in the southwestern US and Heinrich event 1. *Journal of Quaternary Science, 28*(1), 49-58. doi:10.1002/jqs.2586

Ormsby, T. (2010). *Getting to know arcgis desktop for arcgis 10 ; includes exercise data on CD*. Redlands, Calif: ESRI Press.

Rand McNally and Company. (1994) *The new international atlas: 25th anniversary ed*, Chicago: Rand McNally.

Roberts, M. C., Niller, H. -., & Helmstetter, N. (2003). Sedimentary architecture and radar facies of a fan delta, Cypress Creek, West Vancouver, British Columbia. *Geological Society, London, Special Publications, 211*(1), 111-126. doi:10.1144/gsl.sp.2001.211.01.10

Smith, D. L., & Miller, E. L. (1990). Late Paleozoic extension in the Great Basin, Western United States. *Geology, 18*(8), 712. doi:10.1130/0091-7613(1990)0182.3.co;2

Stewart, J. H. (1978). 1: Basin-range structure in western North America: A Review. *Geological Society of America Memoirs,* 1-32. doi:10.1130/mem152-p1

Thomas, D., Nash, D., Shaw, P., & Van der Post, C. (1993). Present day lunette sediment cycling at Witpan in the arid southwestern Kalahari Desert. *CATENA, 20*(5), 515-527. doi:10.1016/0341-8162(93)90045-q

Torgersen, T., De Deckker, P., Chivas, A., & Bowler, J. (1986). Salt Lakes: A discussion of processes influencing palaeoenvironmental interpretation and recommendations for future study. *Palaeogeography, Palaeoclimatology, Palaeoecology, 54*(1-4), 7-19. doi:10.1016/0031-0182(86)90115-x

Twidale, C.R. & Campbell, E.M. (2005). Australian Landforms: *Understanding a Low, Flat, Arid and Old Landscape.* Rosenberg Publishing Pty Ltd, Kenthurst, NSW. 336pp.

Van Dam, R. L., Van Den Berg, E. H., Schaap, M. G., Broekema, L. H., & Schlager, W. (2003). Radar reflections from sedimentary structures in the Vadose Zone. *Geological Society, London, Special Publications, 211*(1), 257-273. doi:10.1144/gsl.sp.2001.211.01.21

Wade, T. G., Wickham, J. D., Nash, M. S., Neale, A. C., Riitters, K. H., & Jones, K. B. (2003). A comparison of vector and raster GIS methods for calculating landscape metrics used in environmental assessments. *Photogrammetric Engineering & Remote Sensing, 69*(12), 1399-1405. doi:10.14358/pers.69.12.1399

Zajícová, K., & Chuman, T. (2019). Application of ground penetrating radar methods in soil studies: A Review. *Geoderma, 343*, 116-129. doi:10.1016/j.geoderma.2019.02.024